2.5-D modelling of elastic waves using the pseudospectral method

Takashi Furumura[1,*] and Hiroshi Takenaka[2]

[1]*Faculty of Education, Hokkaido University of Education, Midorigaoka 2-34-1, Iwamizawa, 068, Japan*
[2]*Department of Earth and Planetary Sciences, Kyushu University, Hakozaki 6-10-1, Fukuoka, 812-81, Japan*

SUMMARY

The pseudospectral method is a high-accuracy numerical modelling technique which requires less memory and CPU time than traditional numerical modelling techniques, such as finite difference. However, full 3-D modelling is still computationally intensive. As we must compromise between realism and computational efficiency, we have developed a 2.5-D pseudospectral scheme for calculating 3-D elastic wavefields in media varying in two dimensions. To demonstrate the feasibility of the scheme described in this paper, we use data from a refraction survey carried out in 1984 by the Explosion Seismology Group in the southeastern foothills of the Hidaka Mountains, Hokkaido, Japan.

Key words: explosion seismology, Hidaka Mountains, synthetic seismograms.

1 INTRODUCTION

The pseudospectral method is an attractive alternative to high-accuracy finite-difference methods that are typically used for numerical modelling of 2-D and 3-D wavefields in heterogeneous media. Since Kosloff & Baysal (1982) applied the pseudospectral method to find the time-domain solution of the seismic wavefield, many numerical techniques have been developed for effectively applying it to actual models: an absorbing boundary (Cerjan et al. 1985; Kosloff & Kosloff 1986; Berg, If & Skovgaard 1990) or a wraparound elimination technique (Furumura & Takenaka 1995); stable differentiation for discontinuous data (Furumura & Takenaka 1992); and mapping techniques to incorporate irregular grid spacing or curved interfaces (e.g. Fornberg 1988; Tessmer & Kosloff 1994; Carcione 1994). For the pseudospectral method, as well as for the finite-difference method, it is straightforward to incorporate anelastic (Witte & Richards 1986; Witte 1989) and anisotropic effects in the scheme.

The main advantage of the pseudospectral method is that it requires several orders of magnitude less computer memory and computation time than other numerical modelling schemes, such as finite difference or finite element. In the pseudospectral method, the field variables are expanded in terms of Fourier interpolation polynomials, and the numerical differentiation of the variables is analytically performed in the Fourier domain (wavenumber domain). This accurate spatial differentiation can reduce memory and computation time by several orders of magnitude as compared with other numerical methods such as the finite-difference or finite-element method.

* On leave at: Research School of Earth Sciences, Australian National University, Canberra ACT 0200, Australia.

For example, for 2-D and 3-D modelling, the memory requirements for the pseudospectral method are about 1/8 and 1/64 of that for the fourth-order finite-difference scheme, respectively (Daudt et al. 1989).

However, even using the pseudospectral method, 3-D elastic modelling has been very expensive because of large memory requirements, so its applications have been restricted to 2-D elastic wavefields (Kang & McMechan 1990) or 3-D acoustic wavefields (Chen & McMechan 1993). 2-D elastic modelling is sometimes conducted for gaining qualitative understanding of wave propagation (e.g. Chen & McMechan 1992; Furumura, Takenaka & Okabe 1993), but the implicit assumption in 2-D modelling, where the source extends infinitely in the out-of-plane direction (i.e. a line-source), results in waveforms and amplitudes which are significantly different from those for a 3-D point-source. 3-D acoustic modelling may provide an approximate P wavefield for an explosion source (P-wave source) in a reflection or refraction survey. However, it may not be adequate because it cannot include the contribution from conversion between P and S waves.

Recently, 3-D elastic modelling by the pseudospectral method has been performed using a supercomputer (Reshef et al. 1988), and parallel computers or workstation clusters (Furumura, Kennett & Takenaka 1995) with sophisticated codes suitable for each machine architecture. Their pioneering work may indicate the arrival of the age of 3-D modelling for elastic wavefields using the pseudospectral method. However, these calculations took a long time, even for very small models. Thus, we believe that it will be a dozen years or so until the 3-D modelling for elastic wavefields can be routinely implemented for realistically large-size models.

An economical approach that does not require the same level of 3-D modelling is to examine the 3-D response of a

model where the material parameters vary only in 2-D geometry. Such a configuration having a 3-D wavefield in a 2-D medium is sometimes called the '2.5-D problem' (e.g. Eskola & Hongisto 1981). Fortunately, the structures in geophysically interesting regions can sometimes be approximated by models in which the heterogeneity patterns are 2-D. Also, most seismic experiments, such as refraction surveys, have been arranged to retrieve 2-D structures under the array of receivers. Therefore, 2.5-D modelling can give reasonable synthetics for actual cases of interest.

2.5-D modelling has been implemented for seismic wave simulation using several approaches: asymptotic ray theory (Bleistein 1986; Bleistein, Cohen & Hagin 1987; Stockewell 1995); the finite-difference method for acoustic wavefields (e.g. Song & Williamson 1995) and elastic wavefields (e.g. Okamoto 1993); the indirect boundary method (e.g. Luco, Wong & De Barros 1990); and the discrete wavenumber boundary-integral equation method (Takenaka, Kennett & Fujiwara 1996). Such 2.5-D schemes can be easily implemented on current computers, since they require storage of almost the same size as the corresponding 2-D calculations.

The aim of the present paper is to propose a 2.5-D pseudospectral scheme for calculating 3-D elastic wavefields in 2-D media. A Fourier transform in the medium-invariant direction is issued to reduce the problem of solving the 3-D equation to that of solving multiple 2-D equations. The 3-D wavefield is synthesized by using an inverse Fourier transform from the wavenumber domain. This can give the waveforms for receivers located out of plane. Since the equations in the 2.5-D scheme are a simple extension of the corresponding 2-D equations, they can be efficiently calculated using numerical techniques developed for 2-D pseudospectral modelling.

In the following section, we give a brief summary of pseudospectral modelling for 3-D elastic wavefields. Next, we derive a 2.5-D pseudospectral scheme through transformation of the 3-D equations. We also show another cost-effective 2.5-D pseudospectral scheme, which is derived for special force systems describing the sources. Then, in order to demonstrate the feasibility of 2.5-D pseudospectral modelling, we implement the 2.5-D scheme for forward modelling of the seismic refraction experiment in the southwestern foothills of the Hidaka Mountains, Hokkaido, Japan, conducted by the Research Group for Explosion Seismology (hereafter called RGES) in 1984 (RGES 1988).

2 3-D PSEUDOSPECTRAL MODELLING OF ELASTIC WAVES

For an isotropic linear elastic medium, the equation of motion in the 3-D rectangular system, where x and y are the horizontal coordinates and z is the vertical one, is given by

$$\rho \ddot{U}_x = \frac{\partial \sigma_{xx}}{\partial x} + \frac{\partial \sigma_{xy}}{\partial y} + \frac{\partial \sigma_{xz}}{\partial z} + f_x,$$

$$\rho \ddot{U}_y = \frac{\partial \sigma_{xy}}{\partial x} + \frac{\partial \sigma_{yy}}{\partial y} + \frac{\partial \sigma_{yz}}{\partial z} + f_y, \tag{1}$$

$$\rho \ddot{U}_z = \frac{\partial \sigma_{xz}}{\partial x} + \frac{\partial \sigma_{yz}}{\partial y} + \frac{\partial \sigma_{zz}}{\partial z} + f_z,$$

where $\sigma_{pq} = \sigma_{pq}(x, y, z, t)$ $(p, q = x, y, z)$ are the stress components at point (x, y, z) at time t; $f_p = f_p(x, y, z, t)$ $(p = x, y, z)$ is the body force; $\ddot{U}_p = \ddot{U}_p(x, y, z, t)$ are the second time deriva-

tives of displacement (i.e. acceleration); and $\rho = \rho(x, y, z)$ is the density. The wavefield radiated from a point source can be included in the equation by using its equivalent body force (e.g. see Aki & Richards 1980, chap. 3). Numerical modelling schemes such as the finite-difference and pseudospectral methods directly compute the discretized versions of the above equations, where the bounded computational domains are usually represented by grids with regular grid spacing. For marching time in the pseudospectral method an explicit scheme is used: the wavefield in the next time step is calculated by use of the current and previous wavefields. For example, the following second-order finite-difference time integration scheme is often used:

$$\dot{U}_p[x, y, z, (n + 1/2)\Delta t] = \dot{U}_p[x, y, z, (n - 1/2)\Delta t] + \ddot{U}_p(x, y, z, n\Delta t)\Delta t, \tag{2}$$

and

$$U_p[x, y, z, (n + 1)\Delta t] = U_p[x, y, z, (n - 1)\Delta t] + \dot{U}_p[x, y, z, (n + 1/2)\Delta t]\Delta t, \tag{3}$$

where $\dot{U}_p$ and U_p $(p = x, y, z)$ denote particle velocity and displacement, respectively, and Δt is the time step. In this time integration scheme, a small Δt is selected to reduce numerical dispersion which arises in the finite-difference approximation of the integration. To keep the dispersion error down to an acceptable level, the criterion of Daudt et al. (1989),

$$\Delta t < 0.26 \frac{\text{Max}(\Delta x, \Delta y, \Delta z)}{V_P^{\max}}, \tag{4}$$

is used, where $V_P^{\max}$ is the maximum P-wave velocity in the model, Δx, Δy and Δz denote constant grid spacings along the x-, y- and z-directions, respectively, and $\text{Max}(\Delta x, \Delta y, \Delta z)$ is the largest among them. The strain components $e_{pq} = e_{pq}(x, y, z, t)$ $(p, q = x, y, x)$ are calculated by the spatial differentiation of the displacement components as follows:

$$e_{pq} = \frac{1}{2}\left(\frac{\partial U_p}{\partial q} + \frac{\partial U_q}{\partial p}\right). \tag{5}$$

The stress and strain components are related through Hook's law with the Lamé's constants $\lambda = \lambda(x, y, z)$ and $\mu = \mu(x, y, z)$ as follows:

$$\sigma_{pq} = \lambda(e_{xx} + e_{yy} + e_{zz})\delta_{pq} + 2\mu e_{pq}, \qquad (p, q = x, y, z), \tag{6}$$

where δ_{pq} is the Kronecker delta. The solution of the full system of equations from (1) to (3), (5) and (6) is marched forward in time after initiation of a seismic disturbance.

Since for the pseudospectral method the spatial differentiation in eqs (1) and (5) is performed analytically in the wavenumber domain, a larger grid spacing can be used than that of the finite-difference method (Fornberg 1987; Daudt et al. 1989). For the pseudospectral method only two grid points per shortest wavelength are theoretically sufficient in the spatial differentiation. The transformation between the physical and wavenumber domains is performed along row and column of the variables to be differentiated using a 1-D fast Fourier transform (FFT). Usually the FFT for complex-valued data (complex-FFT) is used for the spatial differentiation in the pseudospectral method (e.g. Kosloff & Baysal 1982; Reshef et al. 1988). However, the differentiation can be performed more efficiently using the FFT for real-valued data (real-FFT), because both input and output of the transform are purely real-valued data. Note that

the differentiations performed using real FFTs based on sophisticated algorithms are a factor of two faster than performing the differentiations using the complex FFTs (Furumura, Takenaka & Ninomiya 1993).

For the pseudospectral method, numerical techniques for applying the boundary conditions, such as a free surface and an absorbing boundary for a bounded computational region, have also been developed. The free surface can be simply incorporated into the calculation by adding a number of zeros prior to the vertical differentiations of the stress components, or, equivalently, because of the periodicity, below the bottom of the components. When a source is placed near the surface, a large discontinuity at the boundary causes a Gibbs's phenomenon in the vertical derivatives of the displacement. Since this causes an oscillating noise in the wavefield near the free surface, an alternative differentiation scheme for discontinuous data ['symmetric differentiation' (Furumura & Takenaka 1992)] is exploited to suppress the oscillations. An absorbing boundary condition is also applied for the other sides to eliminate wraparound phases due to the implicit periodicity in the FFT. Such unexpected phases can be reduced using the amplitude-tapering technique of Cerjan *et al.* (1985) and its improved scheme (Kosloff & Kosloff 1986; Berg *et al.* 1990). Wraparound phases can also be eliminated efficiently by means of a technique based on an anti-periodic extension of the wavefield (Furumura & Takenaka 1995).

In the next section, we show a 2.5-D equation of motion, which is derived from the 3-D equation and can be solved by the pseudospectral method.

3 2.5-D EQUATION OF MOTION

We now derive a 2.5-D equation of motion for a 3-D wavefield in a 2-D medium that is invariant along one coordinate and varies along the other two coordinates. We assume the medium is invariant in the y-direction throughout the rest of this paper. That is,

$$\lambda = \lambda(x, z), \qquad \mu = \mu(x, z), \qquad \rho = \rho(x, z). \tag{7}$$

We set the y-coordinate of the source position at $y = 0$ without loss of generality.

Then, on performing a Fourier transform of the 3-D equations (1) to (6) with respect to y, we obtain the following 2.5-D equation of motion:

$$\rho \ddot{\tilde{U}}_x = \frac{\partial \tilde{\sigma}_{xx}}{\partial x} + ik_y \tilde{\sigma}_{xy} + \frac{\partial \tilde{\sigma}_{xz}}{\partial z} + \tilde{f}_x,$$

$$\rho \ddot{\tilde{U}}_y = \frac{\partial \tilde{\sigma}_{xy}}{\partial x} + ik_y \tilde{\sigma}_{yy} + \frac{\partial \tilde{\sigma}_{yz}}{\partial z} + \tilde{f}_y, \tag{8}$$

$$\rho \ddot{\tilde{U}}_z = \frac{\partial \tilde{\sigma}_{xz}}{\partial x} + ik_y \tilde{\sigma}_{yz} + \frac{\partial \tilde{\sigma}_{zz}}{\partial z} + \tilde{f}_z,$$

$$\tilde{e}_{pq} = \frac{1}{2}\left(\frac{\partial}{\partial q}\tilde{U}_p + \frac{\partial}{\partial p}\tilde{U}_q\right), \qquad (p, q = x, z),$$

$$\tilde{e}_{yy} = ik_y \tilde{U}_y, \tag{9}$$

$$\tilde{e}_{xy} = \frac{1}{2}\left(\frac{\partial}{\partial x}\tilde{U}_y + ik_y \tilde{U}_x\right),$$

$$\tilde{e}_{yz} = \frac{1}{2}\left(ik_y \tilde{U}_z + \frac{\partial}{\partial z}\tilde{U}_y\right),$$

$$\tilde{\sigma}_{pq} = \lambda(\tilde{e}_{xx} + \tilde{e}_{yy} + \tilde{e}_{zz})\delta_{pq} + 2\mu\tilde{e}_{pq}, \qquad (p, q = x, y, z), \tag{10}$$

where we have used the notation

$$\tilde{g}(x, k_y, z, t) = \int_{-\infty}^{\infty} g(x, y, z, t)\, e^{-ik_y y}\, dy, \tag{11}$$

and the y-invariance of the medium, i.e. eq. (7). Note that the transformed variables, i.e. tilde variables, are generally complex valued. It should also be noticed that, for a fixed value of the wavenumber k_y, these equations depend on only two space coordinates, i.e. x and z. If these equations can be solved, the displacement in the (x, k_y, z) domain (hereafter called the k_y-domain) can be obtained. The displacement in the physical domain, i.e. (x, y, z) domain, can then be derived by inverse Fourier transformation.

For each value of k_y, eqs (8) to (10) can be solved as independent 2-D equations using a 2-D pseudospectral technique, because, due to the invariance with respect to y, there is no coupling between waves of different k_y. The computer memory required for 2.5-D modelling can be reduced down to the same size as that for 2-D modelling, because we do not need to store other k_y components in the memory while we calculate a wavefield for a given k_y. This is the main advantage of 2.5-D modelling compared with 3-D modelling for the reduction of memory resources.

In actual calculations, we must discretize k_y. This discretization can be achieved by assuming the source–medium configuration to be periodic along the y axis. A repetition length L_y along the y axis gives $k_y = n\Delta k_y$, $(\Delta k_y = 2\pi/L_y$; n is an integer). As is often discussed in the modelling by the discrete wavenumber representation method, such as the Aki–Larner technique (Aki & Larner 1970), we can truncate the wavenumber summation near the wavenumber component corresponding to the fundamental Rayleigh wave as

$$\Delta k_y N_y \geq 1.1 \frac{2\pi f^{\max}}{V_S^{\min}}, \tag{12}$$

where the parameters $f^{\max}$ and $V_S^{\min}$ are the maximum frequency and the minimum S-wave velocity in the model (see e.g. Bard & Bouchon 1980). Then we can calculate the $2N_y + 1$ wavefields of $k_y = n\Delta k_y$ ($n = -N_y, \ldots, -1, 0, 1, \ldots, N_y$), but the symmetrical relation of the transformed wavefield,

$$\tilde{U}_p(x, -k_y, z, t) = \tilde{U}_p^*(x, k_y, z, t), \qquad (p = x, y, z) \tag{13}$$

(* represents a complex conjugate), reduces the calculation of the wavefields down to $N_y + 1$.

Finally, these k_y components of the displacement at desired positions, i.e. receiver positions, are converted into the physical domain by using a discrete inverse Fourier transform:

$$U_p(x, y_d, z, t) = \frac{1}{L_y} \sum_{k_y = -N_y\Delta k_y}^{N_y\Delta k_y} \tilde{U}_p(x, k_y, z, t)\, e^{ik_y y_d},$$

$$(p = x, y, z), \tag{14}$$

where the variable y_d denotes the source–receiver distance along the y axis.

Since, as mentioned above, we can considerably reduce the working memory for the 2.5-D computation compared with that for the full 3-D computation, we can easily implement such a program on a workstation or personal computer. The computational time required for the 2.5-D modelling depends on the number of wavenumbers. Of course, the total computational time can be reduced using many computers simultaneously to calculate different k_y components in parallel.

In the next section we show an alternative 2.5-D equation of motion for the wavefields generated by a force system which is symmetric or anti-symmetric with respect to y. The equation can be solved with less memory and time than the scheme described in this section.

4 2.5-D SCHEME OF MOTION FOR A WAVEFIELD EXCITED BY A FORCE SYSTEM THAT IS SYMMETRIC OR ANTI-SYMMETRIC IN Y

In the previous section, we described a general 2.5-D pseudospectral scheme, and showed that it requires less memory to compute the 3-D wavefield in a medium varying in two dimensions than the corresponding 3-D calculation. In eqs (8) to (10), the field variables, such as acceleration, stress, and strain, are transformed into the k_y domain by a Fourier transform with respect to y. Since the transformed variables are then complex-valued, the volume of these data are twice the volume of those in the physical domain. However, if each variable has an even or odd distribution with respect to the coordinate to be transformed (i.e. y), the cosine or sine transform can be used, respectively, instead of the Fourier transform. The transformed variables are then all real-valued. In the case of wavefields excited by a force system that is symmetric or anti-symmetric in y, each variable can be even or odd. This enables us to reduce the computational time and memory to less than half that of the previous complex calculations. In this section we present an alternative 2.5-D equation of motion for calculating the wavefield generated by a force system which is symmetric or anti-symmetric in y. In the following two subsections, we show the 2.5-D pseudospectral schemes corresponding to the two force systems.

4.1 2.5-D pseudospectral scheme for a force system that is symmetric in y

Here we consider the body force system describing a source that is symmetric in the y coordinate, such as that for single forces F_x and F_z, and the moment tensor components M_{xx}, M_{yy}, M_{zz} and M_{xz} and M_{zx}, with all other components being zero. We set the y coordinate of the source position to $y = 0$ without loss of generality. The wavefield excited by this force system is then composed of the even components,

$$U_x(x, y, z, t) = U_x(x, -y, z, t),$$
$$U_z(x, y, z, t) = U_x(x, -y, z, t),$$
(15)

and the odd component

$$U_y(x, y, z, t) = -U_y(x, -y, z, t),$$

all with respect to $y = 0$. These components can be expanded in terms of the cosine functions or sine functions as follows:

$$U_x(x, y, z, t) = \frac{2}{L_y} \sum_{k_y=0}^{N_y \Delta k_y} \tilde{U}_x(x, k_y, z, t) \cos(k_y y),$$

$$U_y(x, y, z, t) = \frac{2}{L_y} \sum_{k_y=0}^{N_y \Delta k_y} \tilde{U}_y(x, k_y, z, t) \sin(k_y y),$$
(16)

$$U_z(x, y, z, t) = \frac{2}{L_y} \sum_{k_y=0}^{N_y \Delta k_y} \tilde{U}_z(x, k_y, z, t) \cos(k_y y),$$

where

$$\tilde{U}_x(x, k_y, z, t) = \int_0^{L_y/2} U_x(x, y, z, t) \cos(k_y y) \, dy,$$

$$\tilde{U}_y(x, k_y, z, t) = \int_0^{L_y/2} U_y(x, y, z, t) \sin(k_y y) \, dy,$$
(17)

$$\tilde{U}_z(x, k_y, z, t) = \int_0^{L_y/2} U_z(x, y, z, t) \cos(k_y y) \, dy.$$

This displacement in the k_y domain, $\tilde{U}_p(x, k_y, z, t) \, (p = x, y, z)$, is real-valued, and subjected to the following set of equations:

$$\rho \ddot{\tilde{U}}_x = \frac{\partial \tilde{\sigma}_{xx}}{\partial x} - k_y \tilde{\sigma}_{xy} + \frac{\partial \tilde{\sigma}_{xz}}{\partial z} + \tilde{f}_x,$$

$$\rho \ddot{\tilde{U}}_y = \frac{\partial \tilde{\sigma}_{xy}}{\partial x} + k_y \tilde{\sigma}_{yy} + \frac{\partial \tilde{\sigma}_{yz}}{\partial z} + \tilde{f}_y,$$
(18)

$$\rho \ddot{\tilde{U}}_z = \frac{\partial \tilde{\sigma}_{xz}}{\partial x} - k_y \tilde{\sigma}_{yz} + \frac{\partial \tilde{\sigma}_{zz}}{\partial z} + \tilde{f}_z,$$

$$\tilde{e}_{pq} = \frac{1}{2} \left(\frac{\partial}{\partial q} \tilde{U}_p + \frac{\partial}{\partial p} \tilde{U}_q \right) \quad (p, q = x, z),$$

$$\tilde{e}_{yy} = k_y \tilde{U}_y,$$

$$\tilde{e}_{xy} = \frac{1}{2} \left(\frac{\partial}{\partial x} \tilde{U}_y - k_y \tilde{U}_x \right),$$
(19)

$$\tilde{e}_{yz} = \frac{1}{2} \left(-k_y \tilde{U}_z + \frac{\partial}{\partial z} \tilde{U}_y \right),$$

$$\tilde{\sigma}_{pq} = \lambda (\tilde{e}_{xx} + \tilde{e}_{yy} + \tilde{e}_{zz}) \delta_{pq} + 2\mu \tilde{e}_{pq} \quad (p, q = x, y, z),$$
(20)

where

$$\tilde{f}_x(x, k_y, z, t) = \int_0^{L_y/2} f_x(x, y, z, t) \cos(k_y y) \, dy,$$

$$\tilde{f}_y(x, k_y, z, t) = \int_0^{L_y/2} f_y(x, y, z, t) \sin(k_y y) \, dy,$$
(21)

$$\tilde{f}_z(x, k_y, z, t) = \int_0^{L_y/2} f_z(x, y, z, t) \cos(k_y y) \, dy.$$

This is a 2.5-D equation of motion with Hooke's law in the k_y-domain for a force system symmetric in y. Note that all variables in this system are real-valued. For each value of k_y, this system can be solved using a 2-D pseudospectral technique, and the solution at desired positions is summed over k_y according to eq. (16) to get the seismograms at those positions. The computational resources of memory and time required in this 2.5-D scheme with real operations are about half those of the previous 2.5-D scheme including complex operations.

4.2 2.5-D pseudospectral scheme for a force system that is anti-symmetric in y

Now we consider another wavefield geometry derived from a force system that is anti-symmetric in y. The 2.5-D scheme for a force system that is anti-symmetric in y is derived in almost the same manner as that for a symmetric force system.

The force system which is anti-symmetric in y, such as for a single force F_y and the moment tensor components M_{xy}, M_{yx}, M_{yz}, and M_{zy}, with all other components being zero, excites a

wavefield that has the odd components

$$U_x(x, y, z, t) = -U_x(x, -y, z, t),$$

$$U_z(x, y, z, t) = -U_z(x, -y, z, t), \tag{22}$$

and the even one

$$U_y(x, y, z, t) = U_y(x, -y, z, t),$$

all with respect to $y = 0$. Then, these can be expanded as

$$U_x(x, y, z, t) = \frac{2}{L_y} \sum_{k_y=0}^{N_y \Delta k_y} \tilde{U}_x(x, k_y, z, t) \sin(k_y y),$$

$$U_y(x, y, z, t) = \frac{2}{L_y} \sum_{k_y=0}^{N_y \Delta k_y} \tilde{U}_y(x, k_y, z, t) \cos(k_y y), \tag{23}$$

$$U_z(x, y, z, t) = \frac{2}{L_y} \sum_{k_y=0}^{N_y \Delta k_y} \tilde{U}_z(x, k_y, z, t) \sin(k_y y).$$

This displacement in the k_y domain, $\tilde{U}_p(x, k_y, z, t)$ $(p = x, y, z)$, is real-valued, and subjected to the following set of equations:

$$\rho \ddot{\tilde{U}}_x = \frac{\partial \tilde{\sigma}_{xx}}{\partial x} - k_y \tilde{\sigma}_{xy} + \frac{\partial \tilde{\sigma}_{xz}}{\partial z} + \tilde{f}_x,$$

$$\rho \ddot{\tilde{U}}_y = \frac{\partial \tilde{\sigma}_{xy}}{\partial x} + k_y \tilde{\sigma}_{yy} + \frac{\partial \tilde{\sigma}_{yz}}{\partial z} + \tilde{f}_y, \tag{24}$$

$$\rho \ddot{\tilde{U}}_z = \frac{\partial \tilde{\sigma}_{xz}}{\partial x} - k_y \tilde{\sigma}_{yz} + \frac{\partial \tilde{\sigma}_{zz}}{\partial z} + \tilde{f}_z,$$

$$\tilde{e}_{pq} = \frac{1}{2}\left(\frac{\partial}{\partial q}\tilde{U}_p + \frac{\partial}{\partial p}\tilde{U}_q\right) \quad (p, q = x, z),$$

$$\tilde{e}_{yy} = -k_y \tilde{U}_y,$$

$$\tilde{e}_{xy} = \frac{1}{2}\left(\frac{\partial}{\partial x}\tilde{U}_y + k_y \tilde{U}_x\right), \tag{25}$$

$$\tilde{e}_{yz} = \frac{1}{2}\left(k_y \tilde{U}_z + \frac{\partial}{\partial z}\tilde{U}_y\right),$$

$$\tilde{\sigma}_{pq} = \lambda(\tilde{e}_{xx} + \tilde{e}_{yy} + \tilde{e}_{zz})\delta_{pq} + 2\mu\tilde{e}_{pq} \quad (p, q = x, y, z), \tag{26}$$

where all variables are real-valued, and

$$\tilde{f}_x(x, k_y, z, t) = \int_0^{L_y/2} f_x(x, y, z, t) \sin(k_y y)\, dy,$$

$$\tilde{f}_y(x, k_y, z, t) = \int_0^{L_y/2} f_y(x, y, z, t) \cos(k_y y)\, dy, \tag{27}$$

$$\tilde{f}_z(x, k_y, z, t) = \int_0^{L_y/2} f_z(x, y, z, t) \sin(k_y y)\, dy.$$

This is a 2.5-D equation of motion with Hooke's law in the k_y domain for a force system which is anti-symmetric in y. The equation can be solved for each k_y by a 2-D pseudospectral technique.

The schemes described in the present and previous subsections can be useful for the 2.5-D modelling when the force system of seismic source is purely symmetric or anti-symmetric in y. However, since any kind of source can be decomposed into a force system that is symmetric and anti-symmetric in y, both schemes proposed in this section can also be used in the case of force systems that are not purely symmetric nor anti-symmetric in the y coordinate, so that the memory required for the computation is reduced by a factor of two, compared with the previous complex scheme.

5   2.5-D PSEUDOSPECTRAL FORWARD MODELLING OF THE 1984 REFRACTION EXPLORATION IN THE SOUTHEASTERN PART OF THE HIDAKA MOUNTAINS

In this section we implement the 2.5-D pseudospectral scheme for forward modelling of a refraction experiment carried out in 1984 in the southeastern part of the Hidaka Mountains, Hokkaido, Japan.

Seismic refraction explorations are usually performed to investigate high-resolution structures along survey lines, where many receivers and some explosion shot points are arranged, and the 2-D structure along the lines is obtained by means of iterative forward modelling of the records. For modelling refraction profiles, a ray-tracing method, rather than full-wave methods such as the finite-difference or pseudospectral method, has generally been used, because its computational time is much less than that for the numerical methods. However, the ray-theoretical approximation does not account for low-frequency effects, so it cannot calculate surface waves and diffracted waves. Thus, we may have to use a full-wave method to revise the model after a preliminary model is obtained by the ray-theoretical method. Recently, Kang & McMechan (1990) used the 2-D pseudospectral method for the iterative forward modelling of the Wichita Uplift–Anadarko Basin region in south-western Oklahoma. They demonstrated the importance of the phase information of both first-arrival and later phases to constrain the model. However, as discussed previously, 2-D modelling cannot give the true amplitude and pulse shape for 3-D point-sources, because no out-of-plane wave-spreading effect is accounted for in the equation. Hence, the 2-D modelling is not appropriate for this purpose.

2.5-D pseudospectral modelling can simulate 3-D wave propagation in a medium varying in two dimensions. We now apply the scheme described in the preceding section to the modelling of the refraction experiment. Since we have no information on source mechanism, source time function, S-wave velocity, density or anelastic constants (Q), we make use of simple assumptions on these unknown parameters. For this reason, the goal of the modelling in this section is to compare the profiles of observed and synthetic seismograms and to demonstrate the feasibility of the 2.5-D pseudospectral method. The correction of the model by iterating the 2.5-D modelling is beyond the aim of this paper.

In the next subsection, we introduce an outline of the explosion experiments (RGES 1988) with a brief review of the geological and geophysical characteristics of the Hidaka region. Then, we perform a 2.5-D pseudospectral modelling. The differences in the seismograms between the 3-D wavefield for a point-source and the 2-D wavefield for a line-source are illustrated in the last subsection.

5.1   1984 seismic refraction exploration in the southeastern foothills of the Hidaka Mountains

Here we summarize the previous studies on geological and geophysical structure of the southeastern foothills of the Hidaka Mountains. In this area lies the Kamuikotan metamorphic belt, which runs across Hokkaido Island from north-west to south-east and reaches the coastline in the Urakawa region. This area includes the aftershock region of the 1982

Urakawa–oki earthquake, M 7.1 (Moriya, Miyamachi & Kato 1983). Fuji & Moriya (1983) showed the existence of thick sediments of considerably slow P-wave velocity ($V_p = 3.6$ km s^{-1}) in this region from a refraction experiment using mining explosion shots. This low V_p anomaly appears to coincide with a low Bouguer anomaly (-150 mgal) in the gravity map of this area compiled by Yamamoto (1987). Studies of the 3-D structure of P-wave velocity (Takanami 1982; Miyamachi & Moriya 1984, 1987) and the anelastic attenuation (Q) factor (Furumura & Moriya 1990) show that very low-velocity (10 per cent or more) and low-Q ($Q \sim 50$) material exists in the Urakawa region, which extends down to 80 km below the free surface.

In 1984, a seismic refraction exploration was carried out by RGES (1988) along a profile from Niikappu to Samani, in the southeastern foothills of the Hidaka Mountains (Fig. 1). This covers a representative part of the 1982 Urakawa–oki earthquake (M 7.1) aftershock region and Kamuikotan metamor-phic belt, which is almost perpendicular to this line. The survey line ranged from 0 to 66 km, oriented approximately perpendicular to the geological strike in order to reduce the off-line effects of 3-D geological heterogeneity. The survey involved five shots of sizes ranging from 400 to 600 kg, and 64 temporary seismic array stations arranged at intervals of about 0.1 km, in which were installed vertical-velocity-type seismometers with a natural period of 2 Hz (Fig. 1). The seismic records were digitized with a resolution of 12 bits and a time sampling increment of 10 ms.

The observed seismic record profile is displayed in Fig. 2. Each trace is plotted in a reduced-time format, $t = T - \Delta/6.0$, where t is the time plotted in s, T is the true traveltime in s, and Δ is the offset between the shot and the receiver in km. Although the receivers were not actually placed exactly on a straight line (see Fig. 1), we simply use the shot–receiver distance as the offset. The plotted amplitude of each trace is normalized by its maximum amplitude to increase the visibility
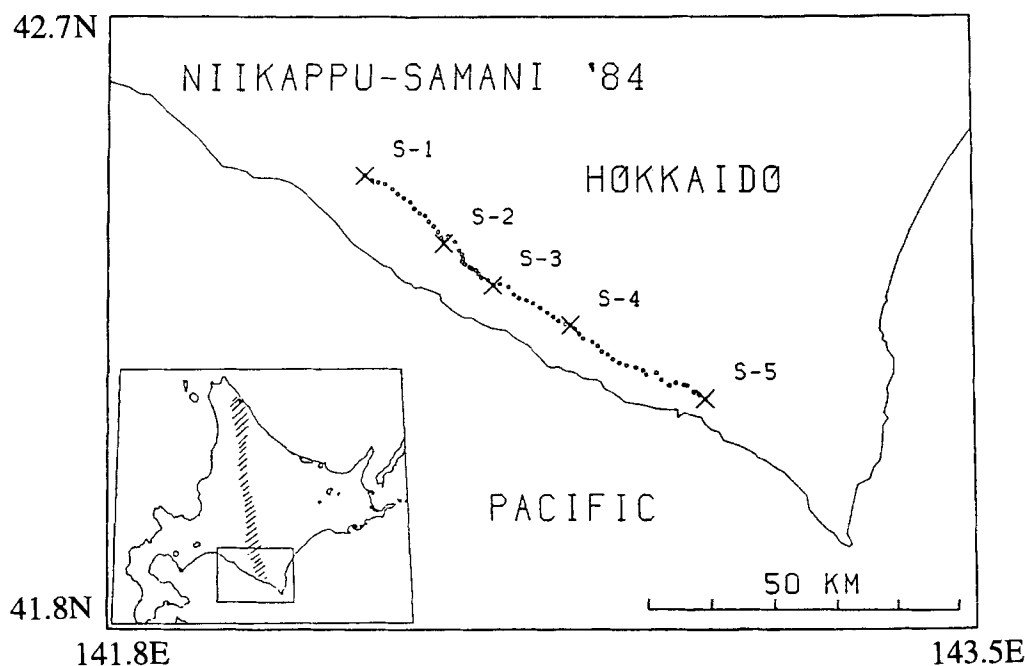

Figure 1. Map showing the location of the 1984 reflection exploration in the southeastern foothills of the Hidaka Mountains, Hokkaido, Japan. Five shots (marked with crosses) and 64 seismic recording stations (small circles) were arranged in the survey line at intervals of about 0.1 km. The hatched area of the inserted map indicates the approximate location of the Kamuikotan metamorphic belt. The survey line was oriented approximately perpendicular to the geological strike. (After RGES 1988.)
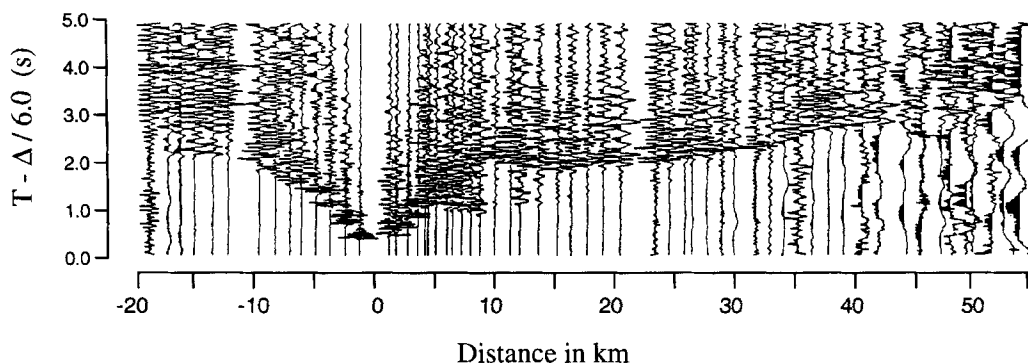

Figure 2. Seismic record profile section of the vertical velocity component for shot S-2. Each trace is normalized by its maximum amplitude. The time axis is plotted in reduced time format with a reduced velocity of 6 km s^{-1}, and the distance for each receiver is measured from the shot point.

of small amplitudes at large distances. The seismic record profile of a shot (S-2) shows a slow apparent velocity of the first arrival and many later phases, which can be considered as reflections, refractions, converted *S*- and surface waves. We also find tentative large-reflection phases following small initial arrivals at the southeastern locations in the distance range 10 to 40 km.

Moriya & RGES (1986) estimated the 2-D *P*-velocity structure along the profile by forward modelling using a ray-tracing method (Fig. 3). This result shows that a sedimentary surface layer of very slow velocity ($V_P = 2.5$ km s^{-1}) and 1 km thickness covers this region, and an inclined high-velocity ($V_P = 5.3$ km s^{-1}) layer lies in the depth range 1 to 6 km from the shot point (S-2) to the end of the survey line.

5.2   2.5-D pseudospectral modelling of the 1984 refraction exploration in the southeastern foothills of the Hidaka Mountains

Now we perform a 2.5-D pseudospectral modelling for the refraction experiment in the southwestern foothills of the Hidaka mountains. Among the five shots, we model a seismic profile of shot S-2, in which we can see many more tentative seismic phases than in the other profiles. We use a 2-D *P*-wave velocity profile estimated by Moriya & RGES (1986), and linearly interpolate the velocity between each layer.

The computational domain is represented by a grid of 512 nodes horizontally by 128 nodes vertically at a regular grid spacing of 0.125 km. We must specify the medium parameters of λ, μ, ρ, at each grid point. We know only the *P*-wave velocity in this model; the *S*-wave velocity and density are unknown. Therefore, we assume the *S*-wave velocity (V_S) profile through the simple assumption of $V_P/V_S = 1.73$, and the density is assumed by means of the following empirical relationship between the *P*-wave velocity (V_P) and the density (ρ), which was proposed by Gregory (1977):

$$\rho = 0.23(3081.5413 V_P)^{1/4}, \tag{28}$$

where the coefficients have been redefined for use with V_P in km s^{-1} and ρ in Mg m^{-3}. An explosion-type point source described by the moment tensor $M_{xx} = M_{yy} = M_{zz} = M_0$ is employed for the numerical modelling, so that we can apply the 2.5-D scheme for the force system which is symmetric in y

described in Section 4.1. We assume the moment of the source as $M_0 = 1$ N m.

In order to avoid one instability problem that arises in the spatial differentiation using the FFT, we use a spatially distributed volume source to produce a band-limited wavefield. An equivalent body force corresponding to the explosion source can then be written as

$$f_x(x, y, z, t) = M_0 \frac{\partial}{\partial x_0} \hat{\delta}(x - x_0, y - y_0, z - z_0, t - t_0)$$

$$= -M_0 \frac{\partial}{\partial x} \hat{\delta}(x - x_0, y - y_0, z - z_0, t - t_0),$$

$$f_y(x, y, z, t) = M_0 \frac{\partial}{\partial y_0} \hat{\delta}(x - x_0, y - y_0, z - z_0, t - t_0)$$

$$= -M_0 \frac{\partial}{\partial y} \hat{\delta}(x - x_0, y - y_0, z - z_0, t - t_0), \tag{29}$$

$$f_z(x, y, z, t) = M_0 \frac{\partial}{\partial z_0} \hat{\delta}(x - x_0, y - y_0, z - z_0, t - t_0)$$

$$= -M_0 \frac{\partial}{\partial z} \hat{\delta}(x - x_0, y - y_0, z - z_0, t - t_0),$$

where $\hat{\delta}$ is a pseudo-delta function for a volume source that has a narrow distribution in space and time around the centre (x_0, y_0, z_0, t_0) of the source, and

$$\int_{-\infty}^{\infty} \int_{-\infty}^{\infty} \int_{-\infty}^{\infty} \int_{-\infty}^{\infty} \hat{\delta}(x, y, z, t) \, dx \, dy \, dz \, dt = 1. \tag{30}$$

In this modelling, we employ the following function, $\hat{\delta}$, as the pseudo-delta function:

$$\hat{\delta}(x, y, z, t) = \bar{\delta}_s(x - x_0)\delta(y)\bar{\delta}_s(z - z_0)\bar{\delta}_t(t - t_0), \tag{31}$$

where we have set the y coordinate of the source position at $y = 0$, i.e. $y_0 = 0$, and $\bar{\delta}_s$ and $\bar{\delta}_t$ are the spatial and time distribution of the source, for which we used Herrmann's pseudo-delta function (Herrmann 1979). Note that for the distribution in the y-direction the Dirac delta function has been used, which will be transformed into k_y-domain through eq. (21). We choose the width of the Herrmann's function as $4\Delta x \times 4\Delta z$ in space; therefore, the source volume extends over 25 grid points in the $x - z$ plane. Substituting eqs (29) and
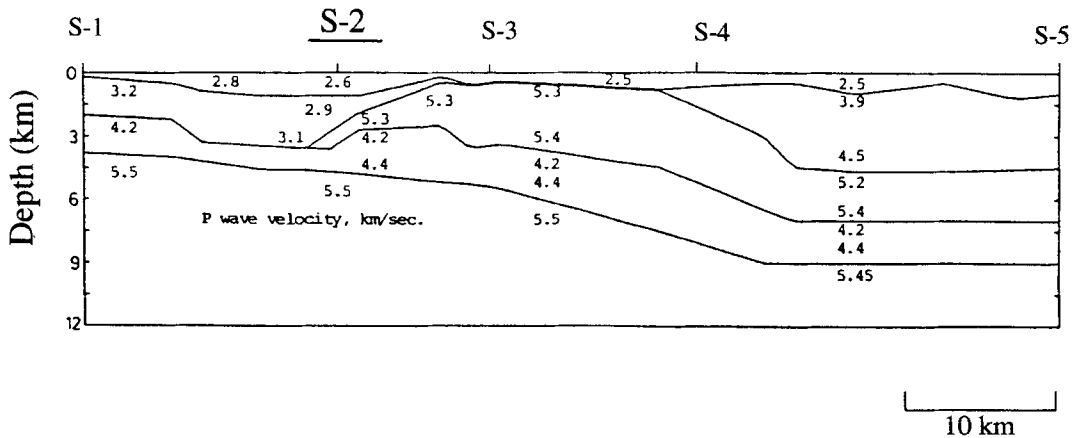

Figure 3. *P*-wave velocity model along the survey line used in the modelling. The numbers within the figure indicate the *P*-wave velocity (km s^{-1}) of the upper and lower boundary of each layer (after Moriya & RGES 1986).

(31) into eq. (21), we get the following representation in the k_y-domain for the equivalent body force to the explosion source:

$$\tilde{f}_x(x, k_y, z, t) = -M_0 \frac{\partial}{\partial x} \bar{\delta}_s(x - x_0)\bar{\delta}_s(z - z_0)\bar{\delta}_t(t - t_0),$$

$$\tilde{f}_y(x, k_y, z, t) = M_0 k_y \bar{\delta}_s(x - x_0)\bar{\delta}_s(z - z_0)\bar{\delta}_t(t - t_0),$$

$$\tilde{f}_z(x, k_y, z, t) = -M_0 \bar{\delta}_s(x - x_0)\frac{\partial}{\partial z}\bar{\delta}_s(z - z_0)\bar{\delta}_t(t - t_0). \quad (32)$$

In the modelling, the source depth (i.e. z_0) corresponds to a half-node below the free surface (62.5 m), since the free surface is assumed in the pseudospectral method to be about a half-node above the uppermost grid point, which agrees well with the actual depth of the shot point (71 m).

The source time function, i.e. $\bar{\delta}_t(t)$ in eq. (31), is also selected to produce a band-limited wavefield. Fig. 4 shows the Fourier spectrum of the waveform recorded 1.3 km from the shot point. Since the frequency range of the observed waveform extends from 2 to 15 Hz, we choose a predominant frequency of 3 Hz for the source.

The absorbing boundary condition of Cerjan *et al.* (1985) is incorporated in the 20 nodes of both the horizontal and the bottom sides in order to reduce the wraparound phases which arise at the sides of the computational domain. A free-surface boundary condition is incorporated in the computation by adding the same number of zeros (128) as the vertical grid size prior to the vertical differentiation of the stress components and discarding them immediately after the differentiation. We also apply the stable Fourier differentiation scheme ('symmetric differentiation') developed by Furumura & Takenaka (1992) for the vertical differentiation of displacement.

We calculated the wavefields of 34 values of k_y (i.e. $k_y = 0$, Δk_y, $2\Delta k_y$, ..., $33\Delta k_y$; $\Delta k_y = 2\pi/L_y \, \text{km}^{-1}$), where we employed
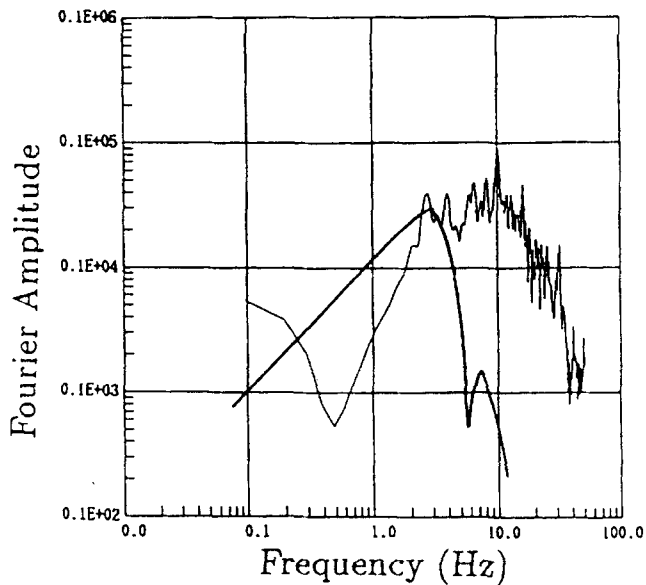

Figure 4. Comparison of the Fourier spectrum of a real seismogram recorded near the source ($\Delta = 1.3$ km) (thin line), and that of the band-limited source time function (centre frequency is 3 Hz) used in the modelling (thick line). Here the source time function has been differentiated with respect to time to display the frequency response of the velocity component.

the spatial periodic length $L_y = 32$ km, which was selected so that the significant wraparound waves would not arrive within the time window of the computation. The number of wavenumbers to be calculated in the modelling was decided using eq. (12). Each calculation was held for 6000 time steps with a time increment of 5 ms to obtain the time window of 30 s. The computation was performed using single-precision arithmetic, and required only 8.4 MB of memory and 4.3 hr of CPU time on a HITAC M-680H main-frame computer (the CPU speed is nearly equal to that of a Sun Microsystems Sparc Station 10 model 40) for one wavenumber (k_y) calculation, so it took 146.2 hr to calculate 34 k_y components. Although we calculated all k_y components sequentially on one computer, the calculation for different k_y s can be performed in parallel using many computers.

5.3 Interpretation of the synthetic seismograms

Fig. 5 displays the 2.5-D synthetic waveforms of vertical and radial velocity components at the in-plane ($y = 0$) receivers. The plotted amplitude of each trace is normalized by its maximum amplitude to increase the visibility of small amplitudes at large distances. Since no energy appears on the transverse components for this calculation, we omitted the transverse components from the figure.

Fig. 6 shows the low-pass-filtered waveforms of the observed seismograms with the cut-off frequency of 6 Hz. Comparison between the synthetic (Fig. 5) and the filtered (Fig. 6) seismograms shows fairly good agreement in first arrivals, later phases, and surface waves. In both real and synthetic seismograms in the distance range of 10 km to 40 km we can see a small first-arriving phase followed by a large phase, which may be the P-wave reflection from the interface between the sediment ($V_P = 2.5$ km s^{-1}) and the rock ($V_P = 5.3$ km s^{-1}).

On the other hand, there are two differences between the real and synthetic profiles.

(1) The polarity of the reflected wave does not agree with that of the real data at distances of more than 20 km.

(2) First arrivals with large amplitudes, which are recorded in the distance range 4 km to 8 km at a time of 1.2 s, do not appear in the synthetic seismograms.

These discrepancies may be mainly due to some minor errors in the P-wave velocity structure of the supposed model.

We find that the polarity of the first-arriving phase in the radial seismograms changes at an offset of -5 km, while this is not observed in the vertical seismograms. This suggests that additional information to constrain the model might be provided by radial seismograms if the horizontal components are recorded in the experiment.

Now we also calculate the P-wave seismograms, U_P, and the in-plane ($y_d = 0$) SV-wave seismograms, U_{SV}, which are defined by the divergence and rotation of the displacement (U_x, U_y, U_z), respectively, as

$$U_P = \frac{\partial}{\partial x} U_x + \frac{\partial}{\partial y} U_y + \frac{\partial}{\partial z} U_z, \quad (33)$$

$$U_{SV} = \frac{\partial}{\partial x} U_z - \frac{\partial}{\partial z} U_x, \quad (34)$$

(Fig. 7). In Fig. 7, only the seismograms of $|\Delta| \leq 15$ km are displayed, because high-frequency noise on the decomposed
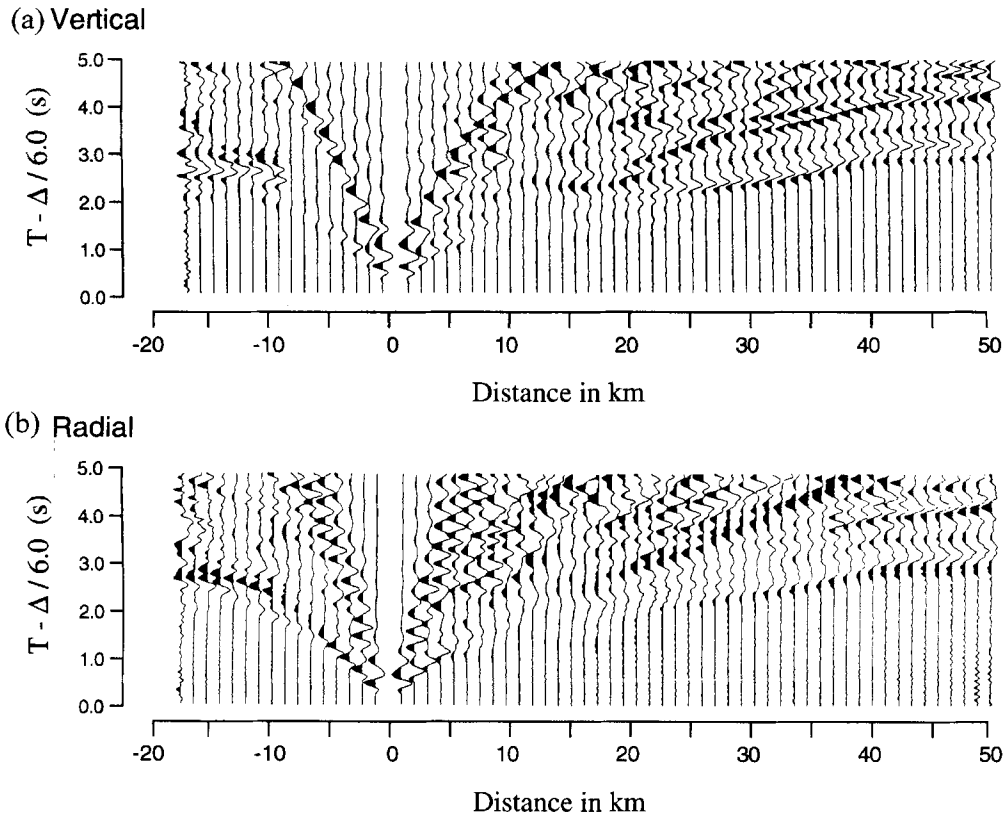
(a) Vertical

(b) Radial

Figure 5. Synthetic velocity seismograms for the shot (S-2) of (a) vertical and (b) radial components. Each trace is normalized by its maximum amplitude. The scales of time and distance axes are the same as in Fig. 2.
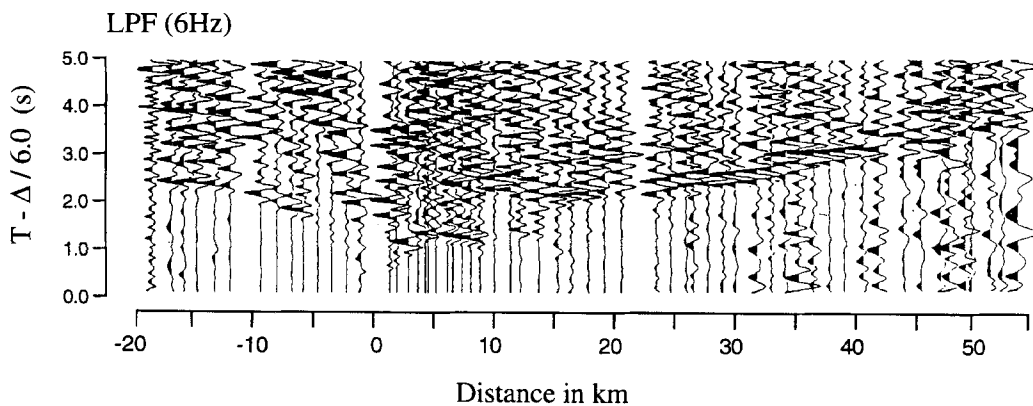
LPF (6Hz)

Figure 6. Seismograms processed by a low-pass filter (with centre frequency of 6 Hz) applied to the real profile (Fig. 2).

seismograms was enhanced due to the spatial differentiation, and the signal-to-noise ratio was not good for $|\Delta| > 15$ km. We can clearly see a Rayleigh wave in the SV-wave seismograms (Fig. 7b). In the P-wave seismograms (Fig. 7a), for the receivers between -5 and -15 km, we also recognize the P-wave reflections 2 s behind the primary plane, which have almost the same propagation speed as the primary phase. Although S-wave energy is not radiated from the explosion source, in the SV-wave seismogram we can clearly see SV waves converted from P waves at the free surface near the shot point or interfaces along the path of wave propagation. These decom-

posed seismograms may give us useful information for the interpretation of the seismograms.

We also show the out-of-plane synthetic seismograms 2 km from the survey line (x axis), i.e. $y_d = 2$ km, in Fig. 8. This distance corresponds to a maximum out-of-plane deviation of the winding receiver locations along the survey line. Since no significant differences are found between the in-plane and the out-of-plane seismograms, except that the arrival times are delayed for the out-of-plane seismograms, it seems reasonable to approximate the winding receiver arrangement along the survey line by the linear receiver array based on the actual
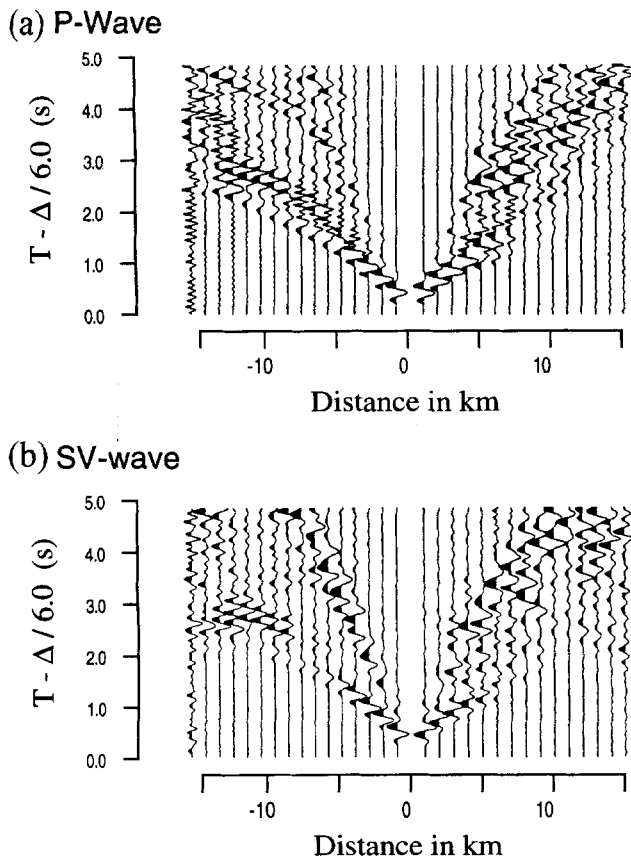
(a) P-Wave

(b) SV-wave

Figure 7. Decomposed seismograms of (a) the *P*-wave component, and (b) the *SV*-wave component. Only the seismograms of near offset ($|\Delta| \leq 15$ km) are displayed, since the signal-to-noise ratio of the seismograms was not good for large offsets.

distance of each receiver from the source. This may be due to the explosive-type source, which isotropically radiates only *P*-wave energy.

5.4 Comparison of 2-D modelling and 2.5-D modelling

In this subsection we compare the waveforms of 2.5-D modelling described in the preceding section and those for the corresponding 2-D calculation. The 2-D synthetics cannot include the true geometrical spreading for 3-D waves, so the phases associated with long ray paths have considerably larger

amplitudes. The amplitudes of waveforms calculated by 2-D modelling may be approximately corrected to get the true amplitudes for 3-D waves by applying a simple scaling function (Kang & McMechan 1990) or by using the 2-D to 2.5-D amplitude correction operator (e.g. Bleistein 1986; Esmersoy & Oristaglio 1988). However, this compensation is not valid unless the heterogeneity of the medium is very small.

Here we illustrate the difference in seismograms between the 3-D wavefield for a point source and the corresponding 2-D wavefield for a line source. The 2-D wavefield can be constructed from the component of $k_y = 0$ in the 2.5-D modelling. We can confirm the difference in waveforms between 2-D modelling (Fig. 9) and 2.5-D modelling (Fig. 5a) on the first arrivals and Rayleigh phase. Fig. 10 shows the enlarged seismograms at offsets of $|\Delta| = 1$, 5, and 15 km, together with their absolute amplitudes. We find that the difference of amplitudes between the 2-D modelling and the 2.5-D modelling increases as the traveltime or source–receiver distance increases.

We also show the amplitude decay curves of the first-arrival phase for 2.5-D and 2-D modelling against distance (Fig. 11). In Fig. 11, the amplitudes of the synthetic and observed waveforms are scaled so as to match each other at $|\Delta| = 2$ km because we cannot estimate the absolute value of the source energy. We can see that the amplitude decay curve of the 2.5-D modelling simulates the observed one well. Also, Fig. 11 shows that it may be difficult to obtain the correct 3-D wave amplitude from the 2-D amplitude by the compensation technique as mentioned above, since the relation between the 2-D and the 3-D amplitudes is not simple in Fig. 6. A difficulty like this using compensation based on a simple filtering process (e.g. Bleistein 1986) in getting the correct 3-D amplitudes and waveforms from the corresponding 2-D calculation is discussed in Song & Williamson (1995).

The discrepancy between the amplitude decay curves for the observed and the 2.5-D synthetic seismograms, which can be seen at the left side of the source position, may be due to the imperfect *P*-wave velocity model and incorrect assumptions of the *S*-wave velocity and the density. We may also have to incorporate an anelastic attenuation (Q) effect in the model to explain the rapid decay of the observational curve, because the study on the 3-D Q structure shows very low Q values in this region (Furumura & Moriya 1990). It is possible to include an anelasticity in the time-domain computation by means of a simple modification of the stress–strain relation (Emmerich & Korn 1987; Witte 1989), although the additional
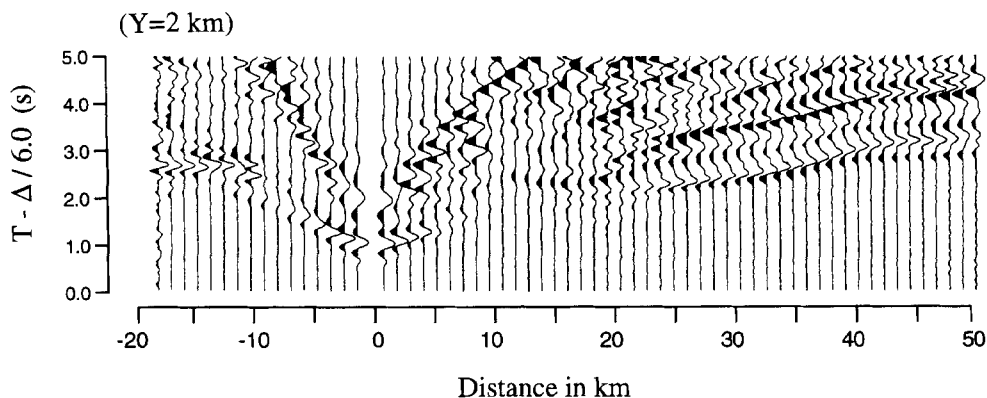
(Y=2 km)

Figure 8. Synthetic velocity seismograms of the vertical component for receivers arranged 2 km from the survey line ($y_d = 2$ km).
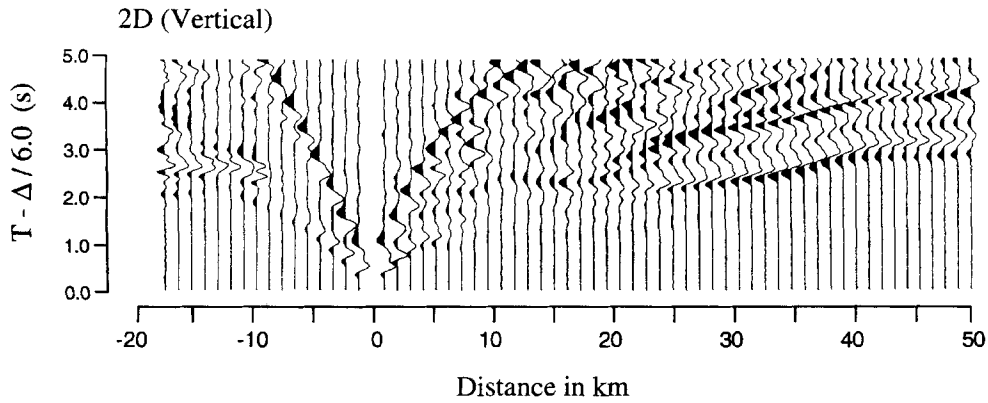
2D (Vertical)

Figure 9. Synthetic velocity seismograms of 2-D modelling, which were synthesized by using a $k_y = 0$ wavefield.
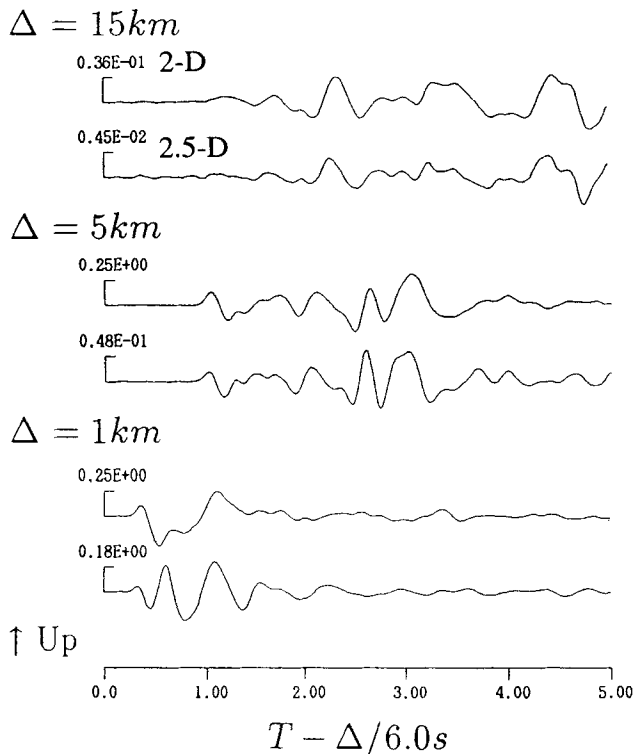

Figure 10. Comparison of the waveforms of the vertical velocity component for three distances ($\Delta = 1$, 5 and 15 km), which were calculated by 2-D (upper trace) and 2.5-D (lower trace) modelling. Each trace is normalized by its maximal amplitude and the scales are shown on the left-hand side of each trace.

computation of the stress–strain history requires much memory and time. These unknown parameters may be obtained by iterative forward modelling, because the amplitudes of the *P* wave depend on the density and *Q* values, as well as *P*-wave velocity, and because the later phases, such as *P*-to-*SV* converted waves and surface waves are affected most by *S*-wave velocity.

6 CONCLUSION

We have presented a 2.5-D pseudospectral method for computing 3-D elastic wavefields in media varying in two dimensions. This method can calculate 3-D wavefields without huge com-
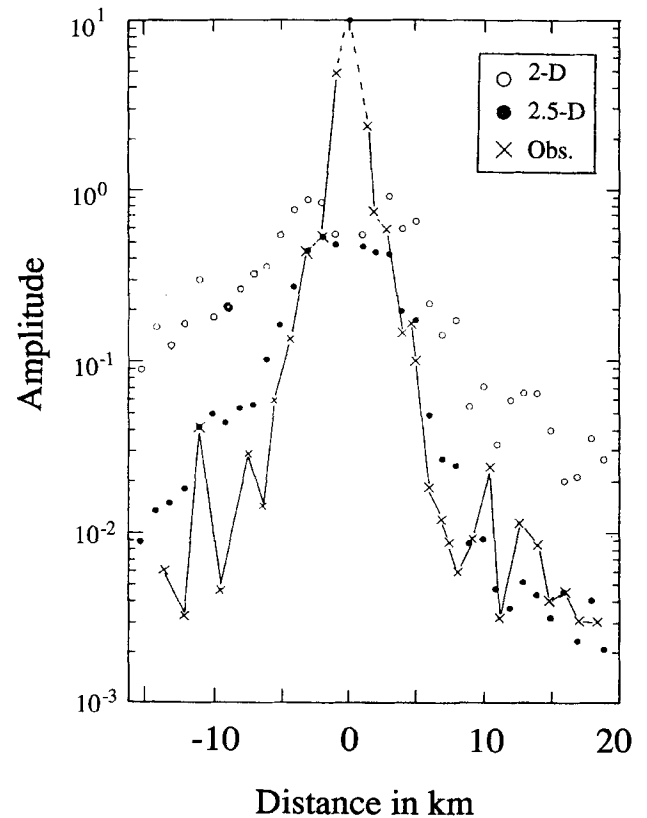

Figure 11. Amplitude-decay-versus-distance curve of the initial phase calculated by 2-D modelling (open circles) and 2.5-D modelling (solid circles). The amplitude measured from the low-pass-filtered seismograms are also plotted on the figure (crosses with line). Each amplitude of the curve is normalized at an offset of 2 km, since the absolute value could not be estimated from the saturated record near the shot point. Note that the amplitude decay curve of the 2.5-D modelling agrees fairly well with the observations, but the 2-D modelling usually overestimates the amplitude at large distance.

puter memory requirements, since it requires storage of the same size as the corresponding 2-D calculations. We have described three kinds of schemes for the 2.5-D pseudospectral method:

(1) the scheme including complex-number operations for a general point source;

(2) the scheme with real-number operations for a source which is symmetric in *y*;

(3) the scheme with real-number operations for a source which is anti-symmetric in *y*.

The second and third schemes work with about half the memory and CPU time required by the first scheme. Since any kind of source can be decomposed into force systems which are symmetric and anti-symmetric in *y* and represented as a linear combination of them, the second and third schemes can also be used in the case of a source that does not have simple symmetry and anti-symmetry in the *y* coordinate.

We have performed 2.5-D pseudospectral modelling for the 1984 refraction survey of the southwestern foot of the Hidaka Mountain, Hokkaido, Japan. Since in this experiment the survey line was extended almost perpendicular to the geological boundary, the 2.5-D configuration can be a fairly good approximation of the actual structure. The results of 2.5-D modelling agreed well with the observed seismograms. Discrepancies of amplitude and polarity between the observed and synthetic seismograms can provide a constraint on the model parameters. In this application of the proposed method, we have employed the isotropic *P*-wave source (explosion source), but the scheme can be readily applied to model seismic waves excited by natural earthquake sources, which generally have a non-isotropic radiation pattern. One of the most significant advantages of the 2.5-D approach is that it is possible for us to take into account the 3-D radiation pattern from the source.

REFERENCES

Aki, K. & Larner, K., 1970. Surface motion of a layered medium having an irregular interface due to incident plane SH waves, *J. geophys. Res.*, **75**, 934–954.

Aki, K. & Richards, P., 1980. *Quantitative Seismology: Theory and Methods*, Freeman & Co., San Francisco, CA.

Bard, P.-Y. & Bouchon, M., 1980. The seismic response of sediment-filled valleys Part 1. The case of incident SH waves, *Bull. seism. Soc. Am.*, **69**, 1–15.

Berg, P., If, F. & Skovgaard, O., 1990. A spectral method for seismic wave propagation in elastic media, *Wave Motion*, **12**, 415–427.

Bleistein, N., 1986. Two-and-one-half dimensional in-plane wave propagation, *Geophys. Prospect.*, **34**, 686–703.

Bleistein, N., Cohen J.K. & Hagin, F.G., 1987. Two and one-half dimensional Born inversion with an arbitrary reference, *Geophysics*, **52**, 26–36.

Carcione, J.M., 1994. The wave equation in generalized coordinates, *Geophysics*, **59**, 1911–1919.

Cerjan, C., Kosloff, D., Kosloff, R. & Reshef, M., 1985. A nonreflecting boundary condition for discrete acoustic and elastic wave equations, *Geophysics*, **50**, 705–708.

Chen, H.-E. & McMechan, G.A., 1992. Computation of multi-attribute seismic wavefields by solution of the elastodynamic equations, *Bull. seism. Soc. Am.*, **82**, 1134–1143.

Chen, H.-E. & McMechan, G.A., 1993. 3-D physical modeling and pseudospectral simulation of seismic common-source data volumes, *Geophysics*, **58**, 121–133.

Daudt, C.R., Braile, L.W., Nowack, R.L. & Chiang, C.S., 1989. A comparison of finite-difference and Fourier method calculations of synthetic seismograms, *Bull. seism. Soc. Am.*, **79**, 1210–1230.

Emmerich, H. & Korn, M., 1987. Incorporation of attenuation into time-domain computations of seismic wave field, *Geophysics*, **52**, 1252–1264.

Eskola, L. & Hongisto H., 1981. The solution of the stationary electric field strength and potential of a point current source in a $2\frac{1}{2}$-dimensional environment, *Geophys. Prospect.*, **29**, 260–273.

Esmersoy, A.C. & Oristaglio, A.M., 1988. Reverse-time wavefield extrapolations, imaging, and inversion, *Geophysics*, **53**, 920–931.

Fornberg, B., 1987. The pseudospectral method: Comparisons with finite differences for the elastic wave equation, *Geophysics*, **52**, 483–501.

Fornberg, B., 1988. The pseudospectral method: Accurate representation of interfaces in elastic wave calculations, *Geophysics*, **53**, 625–637.

Fujii, S. & Moriya, T., 1983. Upper crustal structure in the Hokkaido district by reflection measurements using the quarry blasts, *Geophys. Bull. Hokkaido Univ.*, **42**, 169–190 (in Japanese with English abstract).

Furumura, T., 1992. Studies on the pseudospectral method for the synthetic seismograms, *PhD thesis*, Hokkaido University, Japan (in Japanese).

Furumura, T. & Moriya, T., 1990. Three-dimensional Q structure in and around the Hidaka Mountains, Hokkaido, Japan, *Zisin (J. SSJ)*, **43**, 121–132 (in Japanese with English abstract).

Furumura, T. & Takenaka, H., 1992. A stable method for numerical differentiation of data with discontinuities at end-points by means of Fourier transform-symmetric differentiation, *Butsuri-Tansa (J. SEGJ)*, **45**, 303–309 (in Japanese with English abstract).

Furumura, T. & Takenaka, H., 1995. A wraparound elimination technique for the pseudospectral wave synthesis using an anti-periodic extension of the wavefield, *Geophysics*, **60**, 302–307.

Furumura, T., Takenaka, H. & Ninomiya, I., 1993. Is the fast Hartley transform more efficient than FFT?, *Trans. Jpn. Soc. Indust. appl. Math.*, **3**, 245–255 (in Japanese with English abstract).

Furumura, T. Takenaka, H. & Okabe, S., 1993. Visualization of seismic elastic wavefield calculated using a numerical modeling method, *Trans. Prog. Sym. SIPJ*, **93**, 27–36 (in Japanese).

Furumura, T., Kennett, B.L.N. & Takenaka, H., 1995. Parallel 3-D pseudospectral simulation of wave propagation by using a Connection machine and workstation-clusters, *Geophysics*, submitted.

Gregory, A.R., 1977. Aspects of rock physics from laboratory and long

data that are important to seismic interpretation, *AAPG Memoir,* **26,** 25–46.

Herrmann, R.B., 1979. SH-Wave generation by dislocation source—A numerical study, *Bull. seism. Soc. Am.,* **69,** 1–15.

Kang, I.B. & McMechan G.A., 1990. Two-dimensional elastic pseudo-spectral modeling of wide-aperture seismic array data with application to the Wichita uplift–anadarko basin region of southwestern Oklahoma, *Bull. seism. Soc. Am.,* **80,** 1677–1695.

Kosloff, R., & Baysal, E., 1982. Forward modeling by a Fourier method, *Geophysics,* **47,** 1402–1412.

Kosloff, R. & Kosloff, D., 1986. Absorbing boundaries for wave propagation problems, *J. Comput. Phys.,* **63,** 363–376.

Luco, J.E., Wong, H.L. & De Barros, F.C.P., 1990. Three-dimensional response of a cylindrical canyon in a layered half-space, *Earthq. Eng. Struct. Dyn.,* **19,** 799–817.

Miyamachi, H. & Moriya, T., 1984. Velocity structure beneath the Hidaka Mountains in Hokkaido, Japan, *J. Phys. Earth,* **32,** 13–42.

Miyamachi, H. & Moriya, T., 1987. Velocity structure and aftershock distribution of the 1982 Urakawa-oki earthquake, *J. Phys. Earth,* **35,** 309–326.

Moriya, T., Miyamachi, H. & Kato, S., 1983. Spatial distribution and mechanism solutions for foreshocks, mainshock and aftershocks of the Urakawa-oki earthquake of March 21, 1982, *Geophys. Bull. Hokkaido Univ.,* **42,** 191–213 (in Japanese with English abstract).

Moriya, T. & RGES (Research Group for Explosion Seismology), 1986. Upper crust structure of the eastern part of the Hidaka Mountains using the explosion seismograms, *Prog. Abst. seism. Soc. Jpn.,* **1,** 291 (in Japanese).

Ninomiya, I. & Hadano, Y., 1985, Numerical calculating library (NUMPAC), *Information Proc.,* **26,** 1033–1042 (in Japanese with English abstract).

Okamoto, T., 1993. Teleseismic synthetics obtained from three-dimen-sional calculations in two-dimensional media, *Geophys. J. Int.,* **112,** 471–480.

Reshef, M., Kosloff, D., Edwards, M. & Hsiung, C., 1988. Three-dimensional elastic modeling by the Fourier method, *Geophysics,* **53,** 1184–1193.

RGES (Research Group for Explosion Seismology), 1988. Explosion seismic observations on the southwestern foot of the Hidaka Mountains, Hokkaido, Japan (Niikappu-Samani profile), *Bull. Earthq. Res. Inst. Univ. Tokyo,* **63,** 273–288 (in Japanese with English abstract).

Song, Z.-M. & Williamson P.R., 1995. Frequency-domain acoustic-wave modeling and inversion of crosshole data; Part I—2.5-D modeling method, *Geophysics,* **60,** 784–795.

Stockwell, J.W., Jr., 1995. 2.5-D wave equations and high-frequency asymptotics, *Geophysics,* **60,** 556–562.

Takanami, T., 1982. Three-dimensional seismic velocity anomalies and their relation to local seismicity, *Zisin (J. SSJ),* **35,** 135–139 (in Japanese).

Takenaka, H., Kennett, B.L.N. & Fujiwara, H., 1996. Effect of 2-D topography on the 3-D seismic wavefield using a 2.5-D discrete wavenumber–boundary integral equation method, *Geophys. J. Int.,* **124,** 741–755 (this issue).

Tessmer, E. & Kosloff, D., 1994. 3-D elastic modeling with surface topography by a Chebyshev spectral method, *Geophysics,* **59,** 464–473.

Witte, D.C., 1989. The pseudospectral method for simulating wave propagation, *PhD thesis,* Columbia University, NY.

Witte, D.C. & Richards, P.G., 1986. Anelastic wave propagation by the pseudospectral method, *EOS, Trans. Am. geophys. Un.,* **67,** 303.

Yamamoto, A., 1987. Bouguer anomaly in Hokkaido (1) in and around Hidaka-Taisetsu region, *Prog. Abst. seism. Soc. Jpn.,* **1,** 107 (in Japanese).